Electrochemical and Spectroscopic Studies on the Oxidation of the *cis*-$(Et_2$-dcbpy$)_2RuX_2$ Series of Photovoltaic Sensitizer Precursor Complexes (Et_2-dcbpy = 2,2′-Bipyridine-4,4′-diethoxydicarboxylic Acid, X = Cl^-, I^-, NCS^-, CN^-)

Georg Wolfbauer, Alan M. Bond,* and Douglas R. MacFarlane*

Department of Chemistry, Monash University, Clayton 3168, Victoria, Australia

Received March 30, 1999

The series of *cis*-$(Et_2$-dcbpy$)_2RuX_2$ (Et_2-dcbpy = 2,2′-bipyridine-4,4′-diethoxydicarboxylic acid, X = Cl^-, I^-, NCS^-, and CN^-) sensitizer precursor complexes have been synthesized directly from the esterified ligand (Et_2-dcbpy) rather than via the acid (H_2-dcbpy) in order to obtain high yields. The Ru^{II}/Ru^{III} oxidation process, which is utilized in photovoltaic cell reactions, has been studied in detail by voltammetric and spectroelectrochemical techniques. The $[(Et_2\text{-dcbpy})_2RuCl_2]^{0/+}$ process represents an example of an ideal reversible one-electron oxidation process. The very high stability of the oxidized complex allowed $[(Et_2\text{-dcbpy})_2RuCl_2]^+$ to be characterized by spectroscopic techniques. The ESR spectrum indicates deviation from axial symmetry, and electronic spectra show the disappearance of both MLCT bands and the appearance of one LMCT band as expected for a metal-based oxidation process. Oxidation processes for the other complexes are considerably more complicated. In the case of $(Et_2\text{-dcbpy})_2RuI_2$ an oxidatively induced ligand elimination process was observed to occur after formation of $[(Et_2\text{-dcbpy})_2RuI_2]^+$ to yield $[(Et_2\text{-dcbpy})_2RuI(Solvent)]^+$ and $[(Et_2\text{-dcbpy})_2Ru(Solvent)_2]^{2+}$ complexes in dimethylformamide and acetonitrile. The rate constants for these reactions were estimated from digital simulation of voltammetric data. When dichloromethane was used as the solvent, formation of the five-coordinate $[(Et_2\text{-dcbpy})_2RuI]^+$ complex was observed. The identity of these complexes formed after the initial one-electron oxidation process was confirmed by electrospray mass spectrometry. Oxidation of $L_2Ru(CN)_2$ is even more complicated than oxidation of L_2RuI_2. Both mono- and polynuclear ruthenium compounds are formed as a result of reactions that occur with the oxidized form of the ligand, cyanogen $(CN)_2$, or its derivatives. Oxidation of $L_2Ru(NCS)_2$ leads to elimination of sulfur from the thiocyanate ligand and to formation of $L_2Ru(CN)_2$.

1. Introduction

Ruthenium(II) polypyridyl complexes have been known for many years. They are characterized by strong metal-to-ligand charge transfer (MLCT) bands in the visible region, which make these compounds highly colored. Several other advantageous photophysical properties, such as long-lived triplet states and other luminescence phenomena,[1−4] explain why ruthenium polypyridyl complexes have been widely used as photosensitizers.[5−9] An important application of these photosensitizers is the conversion of sunlight to electrical or other forms of energy. Currently, most photovoltaic sensitizers are based on ruthenium polypyridyl complexes. For example $[Ru(bpy)_3]^{2+}$ (bpy = 2,2′-bipyridine) is a well-known sensitizer in so-called water splitting systems.[4,10,11] Light-induced excitation of one metal-based electron into one of the ligands is followed by a chemical charge separation and finally reduction of the solvent, water, which will produce the valuable energy source hydrogen.[12] More recently, complexes of the formula $(H_2\text{-dcbpy})_2RuX_2$ (H_2-dcbpy = 2,2′-bipyridine-4,4′-dicarboxylic acid) have become very popular sensitizers for photoelectrochemical cells (PEC).[5,13−16] Introducing carbon acid units onto the bipyridine groups enables more effective attachment to semiconductor surfaces. The replacement of one bipyridine by two halides results in a preferable red shift of the absorbance bands. The combination of a semiconductor with a ruthenium sensitizer results in a very efficient charge separation and the possibility of inexpensive PECs with energy conversion efficiencies of up to 10%.[15,17−20] As would have been expected, photophysical studies[21−25] on these kinds of sensitizers have been extensive. However, perhaps

* Authors to whom the correspondence should be addressed. E-mail: A.Bond@sci.monash.edu.au, D.MacFarlane@sci.monash.edu.au. Fax: ++61-3-99054597.

(1) Sonoyama, N.; Karasawa, O.; Kaizu, Y. *J. Chem. Soc., Faraday Trans.* **1995**, *91*, 437−443.
(2) Krausz, E. *J. Chem. Soc., Faraday Trans. 1* **1988**, *84*, 827−840.
(3) Maness, K. M.; Masui, H.; Wightman, R. M.; Murray, R. W. *J. Am. Chem. Soc.* **1997**, *119*, 3987−3993.
(4) Juris, A.; Balzani, V.; Barigelletti, F.; Campagna, S.; Belser, P.; Zelewsky, A. *Coord. Chem. Rev.* **1988**, *84*, 85−277.
(5) Ruile, S.; Kohle, O.; Pechy, P.; Grätzel, M. *Inorg. Chim. Acta* **1997**, *261*, 129−140.
(6) Haga, M. A.; Ali, M. M.; Koseki, S.; Fujimoto, K.; Yoshimura, A.; Nozaki, K.; Ohno, T.; Nakajima, K.; Stufkens, D. J. *Inorg. Chem.* **1996**, *35*, 3335−3347.
(7) Argazzi, R.; Bignozzi, C. A.; Heimer, T. A.; Meyer, G. J. *Inorg. Chem.* **1997**, *36*, 2−3.
(8) Argazzi, R.; Bignozzi, C. A.; Heimer, T. A.; Castellano, F. N.; Meyer, G. J. *J. Am. Chem. Soc.* **1995**, *117*, 11815−11816.
(9) Mcevoy, A. J.; Grätzel, M. *Sol. Energy Mater. Sol. Cells* **1994**, *32*, 221−227.
(10) Amouyal, E. *Sol. Energy Mater. Sol. Cells* **1995**, *38*, 249−276.
(11) Königstein, C. *J. Photochem. Photobiol. A: Chem.* **1995**, *90*, 141−152.
(12) Lei, Y. B.; Hurst, J. K. *Inorg. Chem.* **1994**, *33*, 4460−4467.
(13) Heimer, T. A.; Bignozzi, C. A.; Meyer, G. J. *J. Phys. Chem.* **1993**, *97*, 11987−11994.
(14) Liska, P.; Vlachopoulos, N.; Nazeeruddin, M. K.; Comte, P.; Grätzel, M. *J. Am. Chem. Soc.* **1988**, *110*, 3686−3687.
(15) Nazeeruddin, M. K.; Kay, A.; Rodicio, I.; Humphrybaker, R.; Muller, E.; Liska, P.; Vlachopoulos, N.; Grätzel, M. *J. Am. Chem. Soc.* **1993**, *115*, 6382−6390.
(16) Argazzi, R.; Bignozzi, C. A.; Heimer, T. A.; Castellano, F. N.; Meyer, G. J. *Inorg. Chem.* **1994**, *33*, 5741−5749.

10.1021/ic990344u CCC: $18.00
Published on Web 08/04/1999

surprisingly, general studies characterizing the nature of the oxidized states of those complexes, which is intrinsically important in understanding the physical properties of photovoltaic cells, are yet to appear, although basic electrochemical studies on the oxidation of $(H_2\text{-dcbpy})_2Ru(NCS)_2$ have been reported recently.[26] Such information is of particular importance in understanding the stability of the oxidized state in photosensitizer applications, high stability being a requirement for a long-lived device, despite the relatively short period of time (<1 μs[27]) over which the oxidized state exists in the device before it is reduced to its original state by a charge mediator (commonly iodide).

Structure 1:

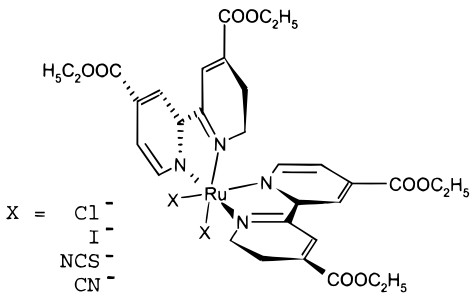

cis-L_2RuX_2

In this paper, a comprehensive electrochemical and spectroscopic study is presented on the oxidation chemistry of the family of ester complexes *cis*-$(Et_2\text{-dcbpy})_2RuX_2$ (Et_2-dcbpy = L = 2,2′-bipyridine-4,4′-diethoxydicarboxylic acid, X = Cl^-, I^-, NCS^-, and CN^-, see structure 1). To the best of our knowledge the complexes with X = I^-, CN^- are novel while the properties of those with X = NCS^-, Cl^- have only been briefly mentioned in the literature,[28−30] and mainly in the context of their use as synthetic precursors. The difference to the complexes commonly used as photovoltaic sensitizers is the esterification of the carbon acid groups, which leads to increased stability and enables simplified procedures to be used in their synthesis.[28,31] The esterified form of the dcbpy ligand is particularly relevant to the photosensitizer applications of $(H_2\text{-dcbpy})_2RuX_2$ compounds, since the carboxylic acid forms a similar ester linkage when attached to the TiO_2 semiconductor electrode.[16,24,32] On exposure to an incident light photon, a metal-based electron from the ruthenium center is promoted into these esterified ligands, hence resulting in generation of a $((-Ti-OOC)_2\text{-bpy}^{\bullet-})Ru$ radical, which then initiates the energy-producing step by injecting the electron into the conduction band of the TiO_2.

2. Experimental Section

2.1. Instrumentation and Procedures. Electrochemical measurements were carried out at (20 ± 2) °C using a standard three-electrode arrangement with a platinum wire as the counter electrode and a Ag/Ag^+ (CH_3CN, 10 mM $AgNO_3$) double-junction reference electrode. The working electrodes were in-house built platinum electrodes of various sizes. A Metrohm 628-10 assembly was used for rotating-disk electrode measurements. CYSY-1 (Cypress Systems) or BAS100 (Bio Analytical System Instruments) electrochemical systems were used to obtain the voltammograms. The DigiSim 2.1 software package (Bio Analytical System Instruments) was used for digital simulation of voltammetric results. The potential of the reference electrode was calibrated against that of the ferrocene/ferrocenium (Fc/Fc^+) redox couple via measurement of the ferrocene oxidation process under conditions (technique, temperature, solvent, and electrolyte) identical with those being used for the compounds of interest. Before each experiment, the electrodes were polished with an aqueous aluminum oxide (0.3 μm) slurry and rinsed with acetone. Oxygen was removed by purging the solutions with high-purity nitrogen or argon.

X-band electron spin resonance (ESR) spectra were recorded with Varian E-12 or Bruker ESP-380 spectrometers. All spectra were measured at 77 K. Gains in the range 1.25×10^2 to 2.5×10^3 and modulation amplitudes around 0.01 and 0.4 mT were typically used. The g values were determined through comparison with the external standard solid diphenylpicrylhydrazyl (DPPH, $g = 2.0037$). Samples were generated ex situ by controlled potential electrolysis experiments at a platinum gauze electrode under an argon atmosphere and transferred, with the exclusion of air, into a nitrogen-degassed quartz ESR tube. Temperature control for ESR experiments was achieved using an ITC4 thermostat (Oxford Instruments Ltd., U.K.).

Optically transparent thin-layer electrolysis (OTTLE) experiments were carried out at 20 °C at a platinum gauze electrode, with a 1 mm quartz cuvette and a Varian Cary 5 near-IR/vis/UV spectrophotometer. The detailed experimental setup is described elsewhere.[33] Mass spectrometric experiments were carried out with a Micromass Platform II (8327E) mass spectrometer, which was equipped with an electrospray coaxial probe as the ion source. Cone voltages were typically in the range 10−50 V, the cone temperature was 55−60 °C, nitrogen was used as the nebulizing gas, and methanol was used as the mobile phase. For experiments involving mass spectrometric examination of bulk electrolyzed solutions, only a 10-fold instead of the usual 100-fold concentration excess of electrolyte (Bu_4NPF_6) was used, in order to minimize signal suppression arising from the electrolyte. All electrolyzed samples also were diluted 1:100 in methanol before commencement of mass spectrometric measurement. For NMR experiments, Bruker AM300 or AC200 instruments were used. All chemical shifts are reported versus an internal TMS standard. ^{13}C spectra reported are proton broad band decoupled. For J-modulated spin-echo experiments a value of $\tau = 7.1$ ms was chosen. Infrared measurements were recorded in Nujol mulls and with a Perkin-Elmer 1600 FT-IR. Elemental analyses were conducted by the Department of Chemistry, University of Otago, Dunedin, New Zealand.

2.2. Solvents and Reagents. Solvents for electrochemical and spectroscopic measurements were of HPLC grade (Mallinckrodt, UltimAR or ChromAR). Dimethylformamide (DMF), as received, contained 0.005% water and was treated with activated 3 Å molecular

(17) Hagfeldt, A.; Didriksson, B.; Palmqvist, T.; Lindstrom, H.; Sodergren, S.; Rensmo, H.; Lindquist, S. E. *Sol. Energy Mater. Sol. Cells* **1994**, *31*, 481−488.
(18) Smestad, G. *Sol. Energy Mater. Sol. Cells* **1994**, *32*, 273−288.
(19) Knödler, R.; Sopka, J.; Harbach, F.; Grünling, H. W. *Sol. Energy Mater. Sol. Cells* **1993**, *30*, 277−281.
(20) O'Regan, B.; Grätzel, M. *Nature (London)* **1991**, *353*, 737−740.
(21) Tachibana, Y.; Moser, J. E.; Grätzel, M.; Klug, D. R.; Durrant, J. R. *J. Phys. Chem.* **1996**, *100*, 20056−20062.
(22) Das, S.; Kamat, P. V. *J. Phys. Chem. B* **1998**, *102*, 8954−8957.
(23) Hannappel, T.; Burfeindt, B.; Storck, W.; Willig, F. *J. Phys. Chem. B* **1997**, *101*, 6799−6802.
(24) Finnie, K. S.; Bartlett, J. R.; Woolfrey, J. L. *Langmuir* **1998**, *14*, 2744−2749.
(25) Rensmo, H.; Sodergren, S.; Patthey, L.; Westermark, K.; Vayssieres, L.; Kohle, O.; Bruhwiler, P. A.; Hagfeldt, A.; Siegbahn, H. *Chem. Phys. Lett.* **1997**, *274*, 51−57.
(26) Bond, A. M.; Deacon, G. B.; Howitt, J.; MacFarlane, D. R.; Spiccia, L.; Wolfbauer, G. *J. Electrochem. Soc.* **1999**, *146*, 648−656.
(27) O'Regan, B.; Moser, J.; Anderson, M.; Grätzel, M. *J. Phys. Chem.* **1990**, *94*, 8720−8727.
(28) Shklover, V.; Nazeeruddin, M. K.; Zakeeruddin, S. M.; Barbe, C.; Kay, A.; Haibach, T.; Steurer, W.; Hermann, R.; Nissen, H. U.; Grätzel, M. *Chem. Mater.* **1997**, *9*, 430−439.
(29) Sprintschnik, G.; Sprintschnik, H. W.; Kirsch, P. P.; Whitten, G. W. *J. Am. Chem. Soc.* **1977**, *99*, 4947−4954.
(30) Haga, M-A.; Bond, A. M. *Inorg. Chem.* **1991**, *30*, 475−480.
(31) Nazeeruddin, M. K.; Pechy, P.; Grätzel, M. *Chem. Commun. (Cambridge)* **1997**, 1705−1706.
(32) Murakoshi, K.; Kano, G.; Wada, Y.; Yanagida, S.; Miyazaki, H.; Matsumoto, M.; Murasawa, S. *J. Electroanal. Chem.* **1995**, *396*, 27−34.
(33) Duff, C. M.; Heath, G. A. *Inorg. Chem.* **1991**, *30*, 2528−2535.

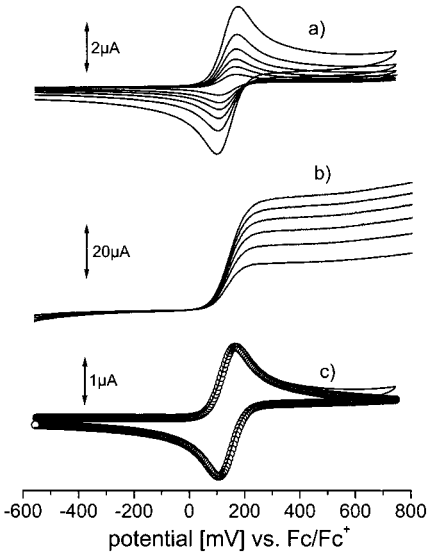

Figure 1. Oxidation of 1.1 mM L_2RuCl_2 in DMF (0.1 M Bu_4NPF_6) under conditions of (a) cyclic voltammetry, υ = 10, 26, 50, 100, 200, and 500 mV s^{-1}, (b) rotating disk electrode, f = 500, 1000, 1500, 2000, 2500, and 3000 min^{-1}, and (c) simulation of a cyclic voltammogram at a scan rate of 100 mV s^{-1} with parameters given in text. Full line: experiment. Circles: simulation.

sieves prior to experiments to reduce the water content. Reagent grade chemicals were used for synthesis of compounds. $RuCl_3 \cdot 3H_2O$ was purchased from Pressure Chemicals Inc. 2,2′-Bipyridine-4,4′-dicarboxylic acid (H_2-dcbpy) was kindly donated by Dr. Leone Spiccia and Prof. Glen B. Deacon.

2.3. Synthesis. Et_2-dcbpy was synthesized by refluxing H_2-dcbpy in C_2H_5OH/H_2SO_4 for 3 days. $RuCl_3$ and Et_2-dcbpy were allowed to react in DMF at 125 °C for $2^1/_2$ hours to give 72% L_2RuCl_2. To obtain the other three complexes, an excess of the corresponding halide salt (KI, NH_4NCS, and KCN) dissolved in water or DMF was added to the former solution and stirring at 80−100 °C undertaken for 1−2 h. In the case of cyanide, de-esterification occurred and the product had to be re-esterified by refluxing the complex in C_2H_5OH/H_2SO_4 for 2 days. The particular details regarding the syntheses, elemental analyses, and spectroscopic characterization (IR and ^1H, ^{13}C NMR) of the ligand and complexes can be found in the Supporting Information. A detailed discussion on the NMR spectra and the syntheses, specifically comparisons to the synthesis of $(H_2\text{-dcbpy})_2Ru(NCS)_2$, is also provided. NMR data confirmed that all L_2RuX_2 complexes were present in the cis configuration, but for convenience the cis prefix will be omitted in further discussion.

3. Results and Discussion

3.1. L_2RuCl_2. (a) Voltammetry and Bulk Electrolysis Experiments in DMF. The voltammetric oxidation of L_2RuCl_2 represents an almost ideal example of a chemically and electrochemically reversible process.

$$L_2RuCl_2 \rightleftharpoons [L_2RuCl_2]^+ + e^- \qquad (1)$$

Figure 1a contains a series of cyclic voltammograms in DMF as a function of scan rate (υ) at a 1 mm diameter platinum macrodisk electrode. The rotated disk electrode voltammograms obtained at the same electrode material are shown as a function of rotation rate (ω) in Figure 1b. Data obtained under a range of conditions are summarized in Table 1. No additional processes are observed up to the solvent limit. Since the voltammetric oxidation of the other compounds is far more complex, data obtained for this system can be conveniently used as a reference.

Table 1. Voltammetric Data Obtained for the Oxidation of 1.1 mM L_2RuCl_2 in DMF (0.1 M Bu_4NPF_6) at 1 mm Diameter and 3 mm Diameter Platinum Macrodisk Electrodes as a Function of Scan Rate or Rotation Rate[a]

Cyclic Voltammetry[b]

υ/mV s^{-1}	E_p^{ox}/mV	E_p^{red}/mV	ΔE_p/mV	$E^r_{1/2}$/mV	i_p^{ox}/i_p^{red}
10	163	103	60	+133	1.02
26	161	101	60	+131	1.01
50	161	107	54	+134	1.00
100	163	103	60	+133	1.00
200	167	101	66	+134	1.00
500	169	97	72	+133	1.00
1000	177	91	86	+134	1.02
2000	187	83	104	+135	1.00
5000	209	59	150	+134	0.99
10000	237	33	204	+135	1.00

Rotating Disk Electrode[c]

f/min^{-1}	slope/mV	$E^r_{1/2}$/mV
500	63	+134
1000	63	+138
1500	65	+141
2000	67	+142
2500	69	+144
3000	69	+146

Microdisk Electrode

r/μm	slope/mV	$E^r_{1/2}$/mV
5.6	60	+133

[a] All peak potentials are reported versus Fc/Fc^+, uncertainty ±2 mV. For CV data, $E^r_{1/2}$ values calculated as $(E_p^{ox} + E_p^{red})/2$; for steady-state techniques, slopes and $E^r_{1/2}$ calculated from "log-plots". υ = scan rate, f = rotation frequency, r = electrode radius, E_p = peak potential, $\Delta E_p = E_p^{ox} - E_p^{red}$, and i_p = peak current. [b] Electrode diameter 1 mm. [c] Electrode diameter 3 mm.

A plot of i_p^{ox} versus $\upsilon^{1/2}$ from cyclic voltammograms (i_p^{ox} = oxidation peak current, υ = scan rate) is linear over the scan rate range 10−5000 mV s^{-1}, implying that the process is diffusion controlled. Mass transport control was also demonstrated via the linear dependency of i_L on $\omega^{1/2}$ (i_L = limiting current, $\omega = 2\pi f$ = angular velocity) in rotating disk electrode experiments. The $E^r_{1/2}$ values (reversible half-wave potential) calculated as $(E_p^{ox} + E_p^{red})/2$ (cyclic voltammetry, E_p^{ox} and E_p^{red} are oxidation and reduction peak potentials, respectively) and from the value of the potential at $i_L/2$ (rotating disk and microdisk electrodes) are given in Table 1. As expected for a reversible process, the $E^r_{1/2}$ value is independent of the voltammetric technique, except when a small contribution from uncompensated resistance is present, as is the case when fast rotation rates are used in rotating disk electrode experiments. Thus the reversible half-wave potential has a value of 133 ± 3 mV vs Fc/Fc^+. Further confirmation of a mass transport controlled reversible one-electron process was obtained from noting that the ratio of i_p^{ox}/i_p^{red} (cyclic voltammetry) was close to unity (Table 1) and that of plots of E versus $\log((i_L - i)/i)$ ("log-plot") had values close to $2.30RT/F$ (58 mV at 22 °C) (rotating disk at slow rotation speeds and microdisk electrode voltammetry, Table 1). The almost completely ideal reversible behavior under the near steady-state conditions present with a microdisk electrode, compared to small departures from ideality with the other techniques, implies that a small contribution from uncompensated resistance is present with techniques based on the use of macrodisk electrodes.

Bulk oxidative electrolysis at a platinum electrode using a controlled potential of 0.5 V required between 15 and 20 min for completion (number of electrons transferred n_{ox} = 1.00 ±

Table 2. Summary of Voltammetric Data Obtained in Different Solvents at 20 ± 2 °C

compound	solvent	D ($\times 10^{-6}$ cm^2 s^{-1})	$E^r_{1/2}$ (mV)
$[L_2RuI(DMF)]^+$	DMF		+460 ± 6
$[L_2Ru(DMF)_2]^{2+}$	DMF		+620 ± 15
$[L_2RuI(CH_3CN)]^+$	CH_3CN		+640 ± 10
$[L_2Ru(CH_3CN)_2]^{2+}$	CH_3CN		+1240 ± 30
$[L_2Ru(CN)(CH_3CN)]^+$	CH_3CN		+810 ± 10
$[L_2RuI]^+$	CH_2Cl_2		+540 ± 15
L_2RuCl_2	DMF	3.1 ± 0.2	133 ± 3
	CH_3CN	7.2 ± 0.2	182 ± 5
	CH_2Cl_2	5.5 ± 0.2	186 ± 3
L_2RuI_2	DMF	3.5 ± 0.3	229 ± 5
	CH_3CN	6.4 ± 0.2	258 ± 4
	CH_2Cl_2	5.8 ± 0.35	226 ± 5
$L_2Ru(NCS)_2$	DMF	*a*	420 ± 20[b]
	CH_3CN	4.4 ± 0.4	470 ± 6
	CH_2Cl_2	6.8 ± 0.2	451 ± 3
$L_2Ru(CN)_2$	DMF	3.5 ± 0.2	603 ± 4
	CH_3CN	7.5 ± 0.5	645 ± 8
	CH_2Cl_2	5.4 ± 0.4	675 ± 10

[a] Multielectron process, see text. [b] Peak potential obtained from differential pulse voltammetry.

0.03). After exhaustive electrolysis, rotating disk and microelectrode voltammograms were identical in slope and $E^r_{1/2}$ value to the values prior to commencing the experiment. However, as expected for a fully reversible system, the voltammetric response was now fully reductive instead of oxidative. Thus, under both short time voltammetric and long time synthetic conditions the reduction process was consistent with the reaction

$$[L_2RuCl_2]^+ + e^- \leftrightharpoons L_2RuCl_2 \qquad (2)$$

On reversing the direction of the bulk electrolysis experiment by applying a potential of 0.0 V, the L_2RuCl_2 complex could be almost quantitatively recovered ($n_{red} = 0.98 \pm 0.03$).

The measured i_L value obtained at a microdisk electrode and the use of eq 3,[34]

$$i_L = 4nFrc^*D \qquad (3)$$

where n is assumed to be exactly 1, F is the Faraday constant, r is the electrode radius, c^* is the bulk concentration, and D is the diffusion coefficient, enabled D to be calculated as 3.1-($\pm$0.2) $\times 10^{-6}$ cm^2 s^{-1}. This value and the measured $E^r_{1/2}$ value (see above) were used to simulate cyclic voltammetric experiments. The result shown in Figure 1c demonstrates that excellent agreement with experimental data is obtained for this very well defined system. $[L_2RuCl_2]^+$ as obtained from a bulk electrolysis experiment in DMF is very stable although after a few hours a very slow color change of the solution from yellow back to green indicates that slow reduction of the oxidized complex occurs to regenerate the starting compound.

(b) Voltammetric Studies in Other Solvents. Studies in acetonitrile and dichloromethane also gave very well defined voltammetric responses, and the reversible $E^r_{1/2}$ values can be found in Table 2. In acetonitrile a second oxidation process is detected just prior to the solvent limit. Under conditions of cyclic voltammetry, the peak potential for this process is located at +1.81 V at a scan rate of 100 mV s^{-1} and the peak current magnitude is similar to that for the preceding initial oxidation process, which indicates that this process may be associated with a one-electron charge transfer step. However, the process does not become fully reversible in the chemical sense under conditions of cyclic voltammetry even when a scan rate of 2000 mV s^{-1} is used. The potential separation of the initial $Ru^{II/III}$ process and this second process is in the range that would be expected if the second process is a $Ru^{III/IV}$ reaction.[35] However, ligand-based oxidation in this very positive potential region cannot be ruled out. Since the focus of this paper is on the $Ru^{II/III}$ process, this second process at very positive potentials in acetonitrile is not further discussed.

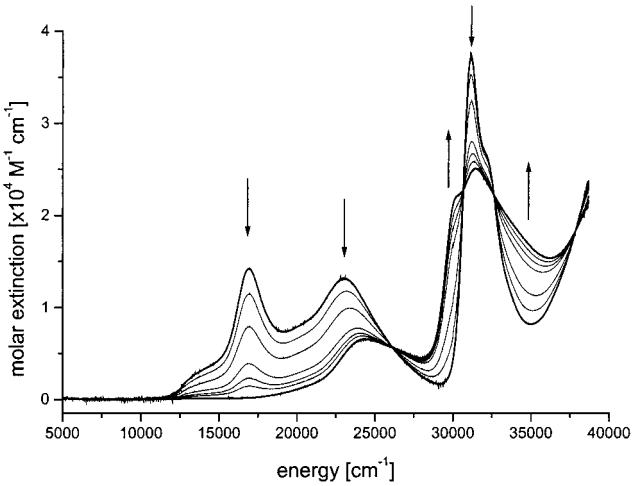

Figure 2. Spectroelectrochemical monitoring of the course of oxidation of 0.7 mM L_2RuCl_2 in an OTTLE electrochemical cell in DMF (0.1 M Bu_4NPF_6).

(c) Spectroelectrochemical Studies. The result of an OTTLE experiment on the oxidation of $L_2Ru^{II}Cl_2$ to $[L_2Ru^{III}Cl_2]^+$ is shown in Figure 2. Four isosbestic points are observed. Reduction of the initially oxidized solution regenerates the electronic spectrum observed with the starting compound. Oxidation of L_2RuCl_2 ($4d^6$) leads to an electron being removed from a metal orbital, resulting in a $4d^5$ configuration (Ru^{III}) and in a collapse of both the MLCT bands present in the spectrum of L_2RuCl_2. However, after oxidation, a chloride lone pair electron is now able to be promoted into the empty t_{2g} metal orbital, resulting in the detection of a ligand-to-metal charge transfer (LMCT) at 24 400 cm^{-1}. This change in electronic spectra is not unusual for metal-based redox processes when the metal changes from a d^6 to a d^5 electron configuration.[36]

(d) ESR Spectrum of $[L_2RuCl_2]^+$. The ESR spectrum of $[L_2RuCl_2]^+$ in frozen DMF is shown in Figure 3. As expected for compounds of this symmetry, parallel and perpendicular components are found. Both the large line width and splitting between both components are typical for a ruthenium-centered spin. However, the perpendicular component is split into two components ($g_{\perp_a} = 2.610$ and $g_{\perp_b} = 2.397$), which indicates a deviation from true axial symmetry and splitting of the t_2 electron level. For $Ru^{III}(pic)_3$ (Hpic = picolinic acid) a similar pseudoaxial symmetry has been found.[37] DeSimone and Drago[38] reported the ESR signal for $[Ru^{III}(bpy)_3]^{3+}$ and noted a minor deviation from perfect axial symmetry. Unusual quadrupole

(34) Oldham, K. B.; Myland, J. C. *Steady-State Voltammetry*; Acadamic Press Inc.: New York, 1993; Chapter 8, pp 263−308.

(35) Schneider, R.; Justel, T.; Wieghardt, K.; Nuber, B. *Z. Naturforsch., B* **1994**, *49*, 330−336.

(36) Shriver, D. F., Atkins, P. W., and Langford, C. H. *Electronic spectra of complexes*, 2nd ed.; Oxford University Press: Oxford, 1996; Chapter 14, pp 579−617.

(37) Ghatak, N.; Chakravarty, J.; Bhattacharya, S., *Polyhedron* **1995**, *14*, 3591−3597.

(38) DeSimone, R. E.; Drago, R. S. *J. Am. Chem. Soc.* **1970**, *92*, 2343−2352.

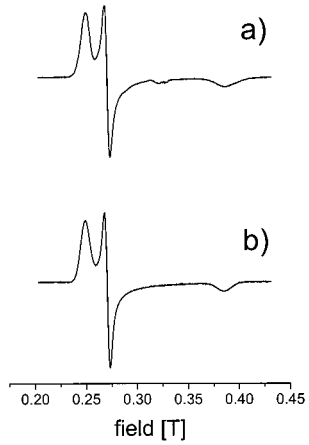

Figure 3. ESR spectrum of $[L_2RuCl_2]^+$ (a) in DMF glass at 77 K, (b) simulated spectrum with $g_{\perp_a} = 2.6103$ ($\Delta H = 8.8$ mT), $g_{\perp_b} = 2.3972$ ($\Delta H = 4.3$ mT), $g_{\parallel} = 1.6801$ ($\Delta H = 14.0$).

splitting in Mössbauer[39] studies and X-ray adsorption[40] data showed that bipyridine is not such a rigid ligand as is phenanthroline. In bipyridine, both aromatic rings are only connected by a single bond, which allows rotation out of the plane. In contrast, in phenanthroline, both rings are additionally connected via a double bond which increases aromaticity and hence forces both pyridine rings into a single plane. No hyperfine structure due to coupling to ^{14}N is observed, which is an indication of the significant metal character of the redox orbital. Most isotopes of ruthenium have spin $S = 0$. Only two ruthenium isotopes are ESR active, but because of their high spin, $S = {}^5/_2$, and low abundance, their signal, as in the case of $[L_2RuCl_2]^+$, is often not observed.

(e) Electrospray-MS studies on Oxidized Solutions of L_2RuCl_2. The formation of the singly charged oxidized complex after bulk oxidative electrolysis was also detected by electrospray mass spectrometry. The main isotopic peak was found at 772.1 (m/z^+), and the isotopic pattern clearly identified the cationic compound giving rise to the signal as having the chemical composition $[L_2RuCl_2]^+$.

3.2. L_2RuI_2. (a) Voltammetry in DMF. Cyclic voltammograms as a function of scan rate (Figure 4a) show that, in contrast to the case with L_2RuCl_2, the oxidation process is chemically irreversible at slow scan rates (<100 mV s^{-1}), although chemical reversibility is found at scan rates $\upsilon \geq 200$ mV s^{-1}, where i_p^{ox}/i_p^{red} values are close to unity (Table 3). Under conditions where the process is chemically irreversible, a second oxidation process is observed at a potential about 230 mV more positive than the initial process. A third response at +620 mV also is observed at very slow scan rates ($\upsilon < 50$ mV s^{-1}). An analogous second (or third) response is not observed in the shorter time domain rotating disk or microdisk electrode (Figure 4c) experiments. Mass transport control of the initial process at short time domains was confirmed by a linear plot of i_L versus $\omega^{1/2}$ which passed through the origin from rotating disk electrode experiments. Additionally the slope of a plot of $\log((i_L - i)/i)$ versus potential was close (see Table 3) to the theoretical value of 58 mV expected for an electrochemically reversible one-electron transfer process at 20 °C. This latter plot also allows the $E^r_{1/2}$ value to be determined in a fashion similar to that for L_2RuCl_2, and the data obtained are summarized in Table 3.

The detection of additional processes under slow scan rate cyclic voltammetric conditions (Figure 4b) indicates that new

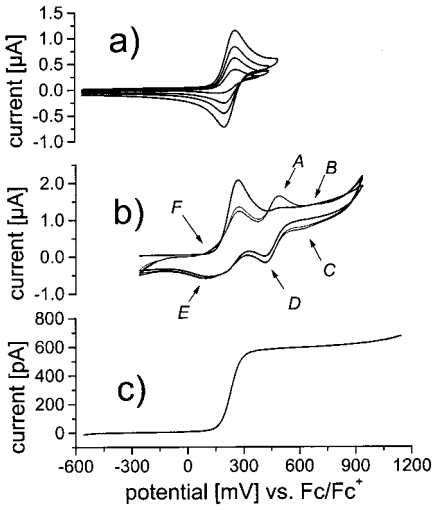

Figure 4. Oxidation of 0.75 mM L_2RuI_2 in DMF (0.1 M Bu_4NPF_6) at a platinum electrode: (a) as a function of scan rate, $\upsilon = 10$, 26, 50, and 100 mV s^{-1}; (b) consecutive scans at $\upsilon = 50$ mV s^{-1}; (c) microdisk electrode $r = 5.6$ μm.

products are formed by a chemical reaction following the charge transfer step which generated $[L_2Ru^{III}I_2]^+$. For other complexes containing easily oxidizable ligands,[41,42] electrochemically generated Ru^{III} complexes have been shown to undergo an internal reaction to produce Ru^{II} and the oxidized ligand.[43] In the particular case of L_2RuI_2 the oxidized form of the ligand is I_2, which itself is electroactive in the potential range of interest.[41,44−46]

The following kind of reaction scheme therefore may be postulated in order to rationalize the electrochemical oxidation of L_2RuI_2:

$$\text{E:} \quad L_2Ru^{II}I_2 \overset{E_1^{o\prime}}{\rightleftharpoons} [L_2Ru^{III}I_2]^+ + e^- \tag{4}$$

$$\text{C}': \quad DMF + [L_2Ru^{III}I_2]^+ \xrightarrow{k_a} [L_2Ru^{II}I(DMF)]^+ + I^\bullet \tag{5}$$

$$\text{C}'': \quad 2I^\bullet \rightarrow I_2 \tag{6}$$

$$\text{E}': \quad [L_2Ru^{II}I(DMF)]^+ \overset{E_2^{o\prime}}{\rightleftharpoons} [L_2Ru^{III}I(DMF)]^{2+} + e^- \tag{7}$$

$$\text{C}''': \quad DMF + [L_2Ru^{III}I(DMF)]^{2+} \xrightarrow{k_b} L_2Ru^{II}(DMF)_2]^{2+} + I^\bullet \tag{8}$$

$$\text{C}'': \quad 2I^\bullet \rightarrow I_2 \tag{9}$$

$$\text{E}'': \quad [L_2Ru^{II}(DMF)_2]^{2+} \overset{E_3^{o\prime}}{\rightleftharpoons} [L_2Ru^{III}(DMF)_2]^{3+} + e^- \tag{10}$$

where $E^{o\prime}$ and k values are the formal reversible potential and rate constant respectively for the relevant reaction. The cyclic voltammetric behavior for this reaction scheme can be readily simulated if the contribution from the highly complex[45] iodine system is omitted (eqs 6 and 9). With this approximation, good

(39) Collins, R. L.; Petit, R.; Baker, W. A. *J. Inorg. Nucl. Chem.* **1966**, *28*, 1001−1010.
(40) Seka, W.; Hanson, H. P. *J. Chem. Phys.* **1969**, *50*, 344−350.
(41) Kotz, J. C.; Vining, W.; Coco, W.; Rosen, R.; Dias, A. R.; Garcia, M. H. *Organometallics* **1983**, *2*, 68−79.
(42) Clark, R. H.; Humphrey, D. G. *Inorg. Chem.* **1996**, *35*, 2053−2061.
(43) Keene, F. R.; Salmon, D. J.; Walsh, J. L.; Abruña, H. D.; Meyer, T. J. *Inorg. Chem.* **1980**, *19*, 1896−1903.
(44) Bhattacharya, S.; Kundu, K. K. *Bull. Chem. Soc. Jpn.* **1989**, *62*, 2676−2683.
(45) Nelson, I. V.; Iwamoto, R. T. *J. Electroanal. Chem.* **1964**, *7*, 218−221.
(46) Datta, J.; Bhattacharya, S.; Kundu, K. K. *Bull. Chem. Soc. Jpn.* **1987**, *61*, 1735−1742.

Table 3. Voltammetric Data Obtained for the Oxidation of L_2RuX_2 in DMF (0.1 M Bu_4NPF_6) at Platinum Electrodes

L_2RuI_2

cyclic voltammetry			rotating disk electrode			microdisk electrode		
v/mV s^{-1}	$E^r_{1/2}$/mV	i_p^{ox}/i_p^{red}	f/min^{-1}	slope/mV	$E^r_{1/2}$/mV	r/μm	slope/mV	$E^r_{1/2}$/mV
10	219	1.95	500	67	229	5.6	65	+232
26	227	1.36	1000	68	232			
50	230	1.17	1500	67	234			
100	230	1.09	2000	66	235			
200	231	1.07	2500	67	237			
500	231	1.02	3000	67	237			
1000	232	1.04						
2000	232	1.04						
5000	234	1.16						

$L_2Ru(CN)_2$

cyclic voltammetry			rotating disk electrode			microdisk electrode		
v/mV s^{-1}	$E^r_{1/2}$/mV	i_p^{ox}/i_p^{red}	f/min^{-1}	slope/mV	$E^r_{1/2}$/mV	r/μm	slope/mV	$E^r_{1/2}$/mV
10	598	1.79	500	72	601	5.6	70	604
26	600	1.63	1000	73	603			
50	601	1.49	1500	73	604			
100	604	1.46	2000	75	605			
200	603	1.20	2500	76	607			
500	604	1.17	3000	75	607			
1000	606	1.12						
2000								
5000								

$L_2Ru(NCS)_2$[a]

cyclic voltammetry	
v/mV s^{-1}	E_p^{ox}/mV
10	530
100	556
500	600

[a] Irreversible oxidation process.

fits between experimental and simulated voltammograms were obtained over the scan rate range 25−1000 mV s^{-1}. Figure 5 shows a comparison of the first five cycles of a cyclic voltammogram obtained by experiment and digital simulation at a scan rate of 500 mV s^{-1}. The best fit to the experimental data over the scan rate range 25−1000 mV s^{-1} was obtained with $k_a = 10^{-1.3\pm0.3}$ s^{-1}, $k_b = 10^{-2.3\pm0.5}$ s^{-1}, $E_1^{\circ\prime} = +0.229$V, $E_2^{\circ\prime} = +0.46$V and $E_3^{\circ\prime} = +0.62$ V. The third electrochemical step, which is attributed to the oxidation of the bis-DMF complex (eq 10) is only visible at very slow scan rates $v = 50$ mV s^{-1} (processes B and C in Figure 4b) in both experimental and simulated digital cyclic voltammograms. The voltammetry of iodine is detected in experimental results and marked as processes F and E in Figure 4b (scan rate 50 mV s^{-1}) but also is almost absent at higher scan rates. (Voltammetric studies on solutions containing I_2 in DMF produce responses E and F.)

(b) Bulk Electrolysis in DMF. Exhaustive controlled potential oxidative bulk electrolysis of a 0.9 mM solution of L_2RuI_2 in DMF at +200 mV ($E^r_{1/2}$ = 229mV) consumes 1.0 ± 0.1 electrons per molecule. The potential used for the electrolysis was chosen to avoid electrochemical oxidation of products formed by reaction of $[L_2RuI_2]^+$ and DMF (eq 5). Traces a and b in Figure 6 show rotating disk voltammograms obtained before and after electrolysis. As expected from data obtained from cyclic voltammograms on L_2RuI_2, on the bulk electrolysis time scale, the mono-DMF-substituted complex, $[L_2RuI(DMF)]^+$, was formed according to eqs 4−6, and it is this complex that gives rise to the reversible oxidative wave at about +460 mV. The preceding wave at ca. +180 mV is due to formation of I_2, the oxidized ligand. However, the iodine is present as a mixture of

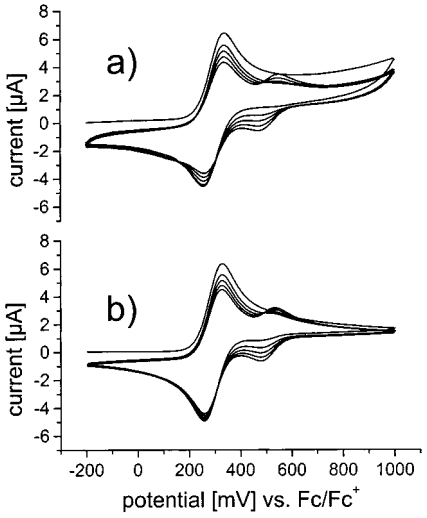

Figure 5. Comparison of experimental and simulated cyclic voltammograms obtained from the oxidation of 2 mM L_2RuI_2 in DMF (0.1 M Bu_4PF_6) at a scan rate of 500 mV s^{-1} with parameters given in text: (a) experiment; (b) simulation.

I_2 and I_3^-, since the potential for bulk electrolysis is close to that expected for the I_2/I_3^- process.

Analysis of plots of $\log((i_L - i)/i)$ versus potential for the oxidation of $[L_2RuI(DMF)]^+$ in DMF obtained from rotating disk voltammograms (500−3000 rpm) after bulk electrolysis yields a slope of 65 ± 3 mV and an $E_{1/2}$ of +0.46 ± 0.01 V. However, the limiting current, i_L, was only moderately reproducible and 85 ± 10% of that of the starting compound,

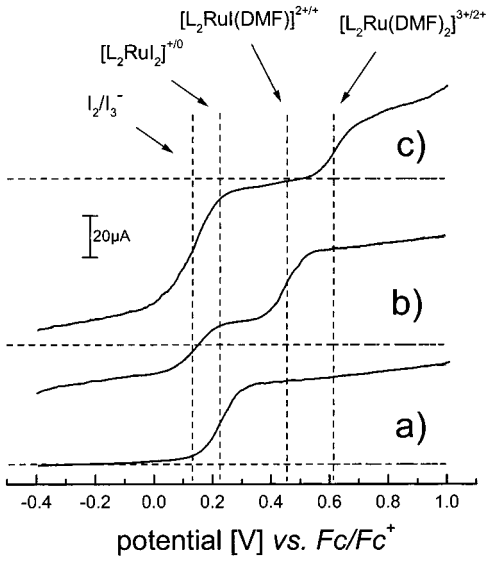

Figure 6. Rotating disk voltammetry (3000 rpm) before and after oxidative bulk electrolysis of 0.9 mM L_2RuI_2 in DMF (0.1 M Bu_4NPF_6). Horizontal dashed lines indicate zero current; vertical dashed lines indicate half-wave potentials. (a) Before electrolysis. (b) After exhaustive electrolysis at +200 mV. (c) After exhaustive electrolysis at +440 mV.

implying that some L_2RuX_2 material has been lost during the course of bulk electrolysis experiments.

Exhaustive oxidative bulk electrolysis at the more positive potential of +440 mV consumed a further 1.1 ± 0.2 electrons per molecule. From eqs 9 and 10 the formation of the bis-DMF complex, $[L_2Ru(DMF)_2]^{2+}$, is expected on this long time scale experiment. A rotating disk voltammogram of the more extensively electrolyzed solution is shown in Figure 6c. The oxidative wave now observed at +0.63 V is associated with the formation of the new $[L_2Ru(DMF)_2]^{2+}$ product. The iodine wave is now fully reductive and double in height relative to that observed after electrolysis at +200 mV as expected when a second equivalent of iodine has been formed as predicted by eq 9. "Log-plot" analysis of data obtained from rotating disk electrode voltammograms for the oxidation of $[L_2Ru(DMF)_2]^{2+}$ gives a slope of 65 ± 5 mV. The limiting current for this process is 80 ± 10% of that of the $[L_2RuI(DMF)]^+$ complex, which implies that loss of L_2RuX_2 material via other unknown reaction pathways also has occurred on the time scale of bulk electrolysis.

(c) ES-Mass Spectrometric Studies on Bulk Electrolyzed Solutions in DMF. Further evidence for the formation of the solvent complexes was obtained using electrospray mass spectrometry. A positive ion mode electrospray mass spectrum of the exhaustive bulk electrolyzed DMF solution of L_2RuI_2 at +200 V is shown in Figure 7a. The major peak occurs at 902.1 m/z^+ and is assigned to a singly charged species which exhibits the typical ruthenium isotopic pattern. Simulation (Figure 7a inset) shows the excellent match with the expected spectrum of the mono-DMF-substituted complex $[L_2RuI(DMF)]^+$. The signal at 861.1 m/z^+ has been identified as arising from $[L_2RuI(CH_3OH)]^+$, where the DMF solvent has been replaced by the methanol solvent introduced when undertaking the mass spectrometric experiments (see Experimental Section). The signal at 1289.4 m/z^+ is due to adduct formation with the Bu_4NPF_6 electrolyte to give $[L_2RuI(DMF)(Bu_4NPF_6)]^+$, and the signal at 1198.3 m/z^+ is assigned to adduct formation of unreacted starting material with the electrolyte cation to give $[L_2RuI_2(Bu_4N)]^+$.

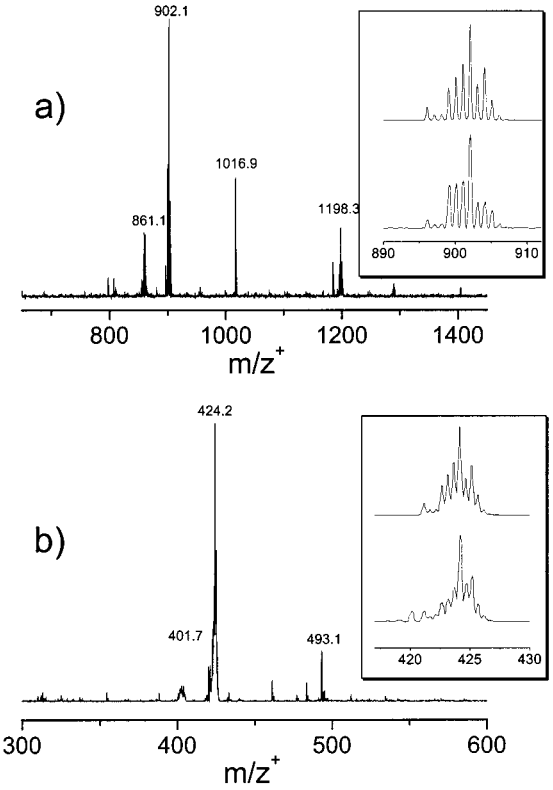

Figure 7. Electrospray mass spectra obtained from bulk oxidatively electrolyzed solutions of L_2RuI_2 in DMF (0.01 M Bu_4NPF_6). After exhaustive electrolysis at (a) +200 mV and (b) +440 mV. Insets show measured (bottom) and simulated (top) spectra of the solvent complexes $[L_2RuI(DMF)]^+$ at 902.1 m/z^+ and $[L_2Ru(DMF)_2]^{2+}$ at 424.1 m/z^+. See text for additional experimental details.

A positive ion mode electrospray mass spectrum of the solution exhaustively electrolyzed at +440 mV is shown in Figure 7b. The main signal is now found at 424.1 m/z^+. Again simulation (Figure 7b inset) provides excellent agreement with the signal expected for the doubly charged bis-DMF-substituted complex $[L_2Ru(DMF)_2]^{2+}$. A weak signal attributable to a doubly charged species with a ruthenium isotope pattern is seen at ca. 403 m/z^+ and is consistent with the spectrum from $[L_2Ru(DMF)(CH_3OH)]^{2+}$. The mass spectrometric results imply that the DMF complexes have considerable stability even in solutions containing a 100-fold excess of CH_3OH.

(d) Studies in Other Solvents. Cyclic voltammograms of L_2RuI_2 in CH_2Cl_2 and CH_3CN gave a well-defined initial metal-centered oxidation in both solvents which is reversible at fast scan rates. However, in both solvents this initial process becomes irreversible at slow scan rates, in which case it is followed by a series of overlapping processes. When the rotating disk or microdisk electrode techniques are used, "log-plot" analysis of the first oxidation process in both solvents under these short time domain conditions again was consistent with a reversible one-electron charge transfer process (Table 2).

Exhaustive bulk electrolysis of L_2RuI_2 at +250 mV in CH_3CN produced the monosubstituted complex $[L_2RuI(CH_3CN)]^+$, although the yield was only about 70%. From rotating disk electrode measurements undertaken on the electrolyzed solution the reversible half-wave potential for the oxidation of $[L_2RuI(CH_3CN)]^+$ was calculated as $E^r_{1/2} = 0.64$V. The singly charged $[L_2RuI(CH_3CN)]^+$ complex was also readily identified from electrospray mass spectrometry since the main signal of a bulk electrolyzed solution was found at 870.1 m/z^+. An additional signal derived from the presence of a singly charged ruthenium

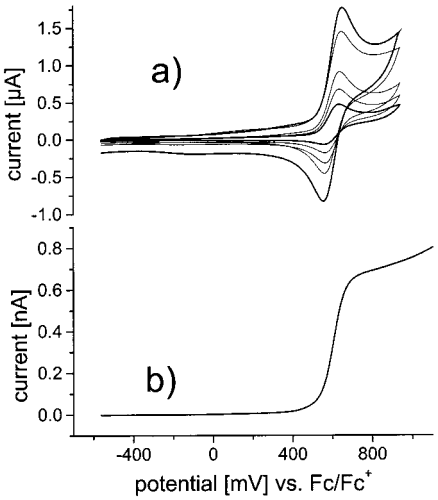

Figure 8. Oxidation of $L_2Ru(CN)_2$ in DMF (0.1 M Bu_4NPF_6): (a) as a function of scan rate at a platinum 1 mm electrode, $\upsilon = 10$, 26, 50, 100, and 200 mV s^{-1}; (b) under near steady-state conditions at a platinum microdisk electrode $r = 5.6$ μm.

compound of unknown identity was observed at 929.3 m/z^+. The signal expected from formation of the CH_3OH-substituted complex, $[L_2RuI(CH_3OH)]^+$, at 861 m/z^+ was not observed in the presence of methanol added prior to undertaking mass spectrometric measurements, indicating that CH_3CN forms even more stable complexes than DMF with this type of ruthenium compound. Bulk electrolysis carried out at a potential of +610 mV formed a low yield of the $[L_2Ru(CH_3CN)_2]^{2+}$ complex. The oxidation wave of this complex was partly overlapped with other unidentified processes, but was determined to have a value of $E_{1/2} = 1.24$ V from rotating disk electrode experiments. The existence of $[L_2Ru(CH_3CN)_2]^{2+}$ was verified from electrospray mass spectra via observation of a signal of a doubly charged ruthenium compound at 392.1 m/z^+.

Oxidative bulk electrolysis of L_2RuI_2 in CH_2Cl_2 at +240 mV proceeded in a manner similar to bulk electrolysis in DMF and CH_3CN and consumed 0.9 ± 0.2 electrons per molecule. After the exhaustive electrolysis, a new oxidation wave at 0.54 ± 0.01 V was observed using rotating disk voltammetry. Electrospray mass spectrometry did not show a signal at 913.0 m/z^+ as expected for the monosubstituted solvent complex $[L_2RuI(CH_2Cl_2)]^+$; rather the main signal was located at 829.0 m/z^+, which is attributable to the formation of the five-coordinate unsubstituted $[L_2RuI]^+$ complex. A signal at 861.1 m/z^+ is assigned to formation of $[L_2RuI(CH_3OH)]^+$. Although there is no direct mass spectrometric evidence for the existence of the monosubstituted CH_2Cl_2 complex $[L_2RuI(CH_2Cl_2)]^+$, it might still be present in the solution phase, since a weakly coordinating solvent molecule of this kind could have been removed in the electrospray process. Alternatively, $L_2RuI(PF_6)$ may be present in dichloromethane solutions containing 0.01 M Bu_4NPF_6 electrolyte.

3.3. $L_2Ru(CN)_2$. (a) Voltammetry and Bulk Electrolysis Experiments in DMF. As was the case with L_2RuI_2, cyclic voltammograms of the cyanide analogue recorded at slow scan rates were not fully reversible until scan rates $\upsilon > 200$ mV s^{-1} were used. Cyclic voltammograms at a platinum macrodisk electrode as function of scan rate are shown in Figure 8, and data are summarized in Table 3. Data obtained from microdisk electrode and rotating disk electrode experiments also may be found in Table 3. Under the latter short time domain conditions the voltammetry showed almost ideal behavior for a reversible one-electron oxidation process. The $E^r_{1/2}$ value for the

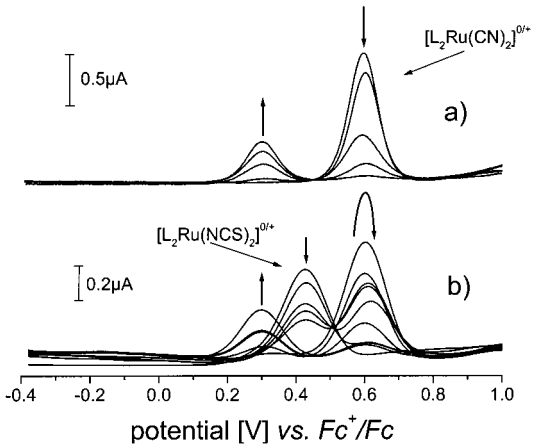

Figure 9. Oxidative bulk electrolysis of $L_2Ru(NCS)_2$ in DMF monitored by differential pulse voltammetry which demonstrates the conversion into $L_2Ru(CN)_2$ and the formation of a new product: (a) 0.9 mM $L_2Ru(CN)_2$, $E_{appl} = +0.50$ V; (b) 1.0 mM $L_2Ru(NCS)_2$, $E_{appl} = +0.27$ V.

$[L_2Ru(CN)_2]^{0/+}$ process was determined to be +0.60 V, which is very much more positive than found for the chloride and iodide derivatives.

The peak potential for oxidation of cyanide present in a 1 mM solution of KCN in DMF (0.1 M Bu_4NPF_6) occurs at +0.63 V ($\upsilon = 200$ mV s^{-1}, platinum electrode). The process is irreversible and very broad and commences at ca. 0.0 V. A mechanism related to that for the oxidation of L_2RuI_2 under conditions where the process is chemically irreversible would lead to the formation of $[L_2Ru(CN)(DMF)]^+$ and $[L_2Ru(DMF)_2]^{2+}$. However, the bis-DMF complex has a reversible half-wave potential of +0.62 V. Thus, when controlled potential electrolysis is used to oxidize $L_2Ru(CN)_2$ ($E^r_{1/2} = +0.60$ V), any $L_2Ru(CN)_2$ would be immediately oxidized to highly reactive $[L_2Ru(DMF)_2]^{3+}$.

Bulk electrolysis of a 0.9 mM $L_2Ru(CN)_2$ solution in DMF (0.1 M Bu_4NPF_6) at a platinum electrode was carried out with $E_{appl} = +500$ mV, which corresponds to the foot of the initial oxidation process and where subsequent oxidation of products formed by EC type processes is expected to be minimized. The exhaustive oxidation of $L_2Ru(CN)_2$ at this potential requires the transfer of two electrons ($n = 2.05 \pm 0.1$) and leads to a color change of the solution from dark purple to pale yellow. The course of the electrolysis was monitored by differential pulse voltammetry (Figure 9a), which reveals the formation of a new product which can be oxidized at +0.30 V. Steady-state microdisk electrode voltammetric techniques showed that this new product was formed in small yields of less than 20%. Upon reduction of the bulk electrolyzed solution at 0 V, the color changed again to dark purple, indicating the formation of a Ru^{II} species.

(b) ES-Mass Spectrometric Studies in DMF. Electrospray mass spectrometric studies on bulk oxidized $L_2Ru(CN)_2$ solutions in DMF initially showed only one major product peak with a typical ruthenium isotopic pattern at 762.6 m/z^+. The peak pattern indicated that this resulted from a doubly charged trinuclear ruthenium species. The fact that the intensity was insensitive to the cone voltage indicates that a compound present in the solution phase produces the spectrum and that it is not from a compound formed in the electrospray source. Furthermore, this response remained after reduction at 0.0 V, so it is not associated with the product that gives the voltammetric process at +0.30 V. After the bulk electrolyzed solution was left to stand for several minutes, the appearance of several new

peaks assigned to bi- and trinuclear ruthenium compounds were seen between 600 m/z^+ and 1600 m/z^+, while the peak at 762.6 m/z^+ disappeared. No ruthenium patterns were found in the negative ion mass spectrum mode. The uncharacterized products formed by electrochemical oxidation of $L_2Ru(CN)_2$ are believed to be complexes formed by reaction with cyanogen,[47] the oxidized form of the ligand $(CN)_2$.

(c) Studies in Other Solvents. In CH_2Cl_2 higher scan rates ($\upsilon > 1000$ mV s^{-1}) are required than in DMF to achieve complete chemical reversibility for the $Ru^{II/III}$ oxidation process. No additional processes are observed for oxidation of $[L_2Ru(CN)_2]^+$ up to the solvent limit at +1.6 V. The voltammetry in CH_3CN is similar, with no additional processes for oxidation of $[L_2Ru(CN)_2]^+$ being observed up to +2.0 V. Oxidative bulk electrolysis of $L_2Ru(CN)_2$ at +605 mV in CH_3CN occurred with the transfer of $n = 0.9 \pm 0.1$ electron per molecule. Rotating disk electrode voltammetric measurements made during the course of electrolysis show the disappearance of the $L_2Ru(CN)_2$ oxidation process and the appearance of a new oxidative wave at 0.89 V. The limiting current at the rotated disk electrode for this wave was only about 30% of that for oxidation of $L_2Ru(CN)_2$. ES-mass spectra show one major peak at 770.3 m/z^+, and the mass distribution indicates that this response arises from a doubly charged binuclear ruthenium species and is consistent with the formula $[L_2Ru(CN)(CH_3CN)]_2^{2+}$.

3.4. $L_2Ru(NCS)_2$. (a) Voltammetry and Bulk Electrolysis Experiments in DMF. Under conditions of cyclic voltammetry, the oxidation of $L_2Ru(NCS)_2$ in DMF was chemically irreversible at all scan rates used up to 10 000 mV s^{-1}. Minor processes following the initial metal-based oxidation are believed to be caused by oxidation of surface-based products, although these processes were less pronounced in DMF than after oxidation of $(H_2\text{-dcbpy})_2Ru(NCS)_2$.[26] Since the oxidation process is not reversible, the $E^r_{1/2}$ value in DMF cannot be calculated and only peak potentials (Table 3) are available. As observed for $(H_2\text{-dcbpy})_2Ru(NCS)_2$,[26] the magnitude of the limiting current per unit concentration obtained via steady-state techniques indicates that the oxidation process corresponds to an $n > 1$ electron process.

Oxidative bulk electrolysis ($E_{appl} = +270$ mV) of 1.0 mM $L_2Ru(NCS)_2$ in DMF yields the corresponding cyanide complex $L_2Ru(CN)_2$ (eq 11). Kohle and co-workers[48] have reported a slow conversion of $(H_2\text{-dcbpy})_2Ru(NCS)_2$ to the cyanide analogue upon illumination. The analogy with electrochemical oxidation is appropriate since a photoexcitation involves a metal-to-ligand charge transfer (MLCT) in which the metal changes from a d^6 to a d^5 electron configuration, which is equivalent to a metal-based oxidation.

$$L_2Ru(NCS)_2 \rightarrow L_2Ru(CN)_2 + \text{oxidized "S"} + ne^- \qquad (11)$$

The number of electrons transferred during the course of the bulk electrolysis was 6 ± 2 electrons per molecule, and the large value is a consequence of oxidation of sulfur, which exists in the oxidation state −2 in thiocyanate and can be oxidized up to +3, depending on the reaction pathway.[49] The transformation described by eq 11 was monitored by differential pulse voltammetry (Figure 9b) during the course of the bulk electrolysis ($E_{appl} = +270$ mV). Prolonged and further oxidation at a potential of $E_{appl} = +500$ mV yielded the same product of unknown identity at 0.30 V as obtained by direct oxidation of $L_2Ru(CN)_2$ (Figure 9a).

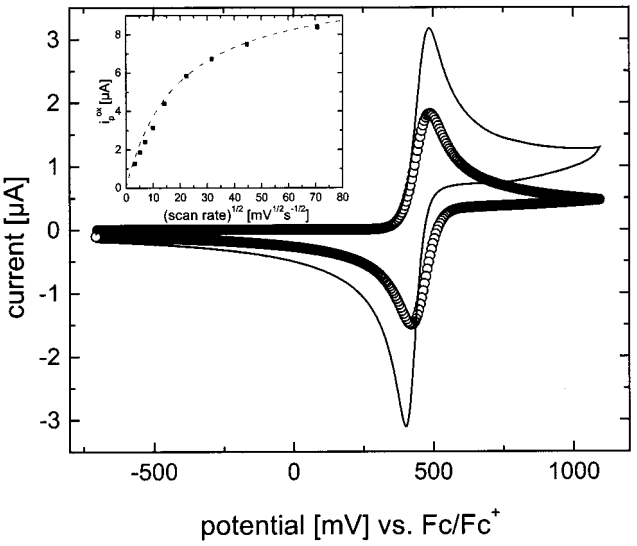

Figure 10. Cyclic voltammograms ($\upsilon = 100$ mV s^{-1}) for the oxidation of 1.0 mM $L_2Ru(NCS)_2$ in CH_2Cl_2 (0.2 M Bu_4NPF_6) at a 1 mm platinum electrode. Full line: measured. Circles: simulated using parameters described in the text. Inset: Anodic peak current (i_p^{ox}) versus $\upsilon^{1/2}$.

It is noteworthy that under no conditions was the formation of the mixed thiocyanate−cyanide complex, $L_2Ru(NCS)(CN)$, observed. Assuming ligand additivity,[33,50] the potential for this complex would be expected to lie between those for the thiocyanate and cyanide complexes at +0.51 V. However, even when the applied oxidation potential for the thiocyanate complex was set at +0.27 V, only the formation of the bis cyanide complex was observed. This result implies that the sulfur elimination reaction may occur via formation of a cyclic intermediate and some form of rearrangement, as the thiocyanate ligand flips from N bond to C bond after the loss of sulfur. Crystallographic data[28] report an angle of 86° between both NCS groups and the near linearity of the NCS groups, which indicate that both thiocyanate groups are in close vicinity. If a metal centered oxidation occurs initially and the partly vacant t_{2g} orbital is filled by an electron from one of the thiocyanate ligands, the NCS group would lose its linear structure and the terminal sulfur could bend and interact with the other NCS group. The thiocyanate ligands are thermodynamically capable of reducing the Ru(III) center, since free thiocyanate can be oxidized at a lower potential than $L_2Ru(NCS)_2$.[26] Transition products are probably associated with the surface-based phenomena, not observed with the other complexes. The large number of post waves, especially at low temperatures (5 superimposed post waves following the initial oxidation process can be observed in acetone at −60 °C), implies that a very complex reaction pathway is associated with the conversion of $L_2Ru(NCS)_2$ to $L_2Ru(CN)_2$.

(b) Studies in Other Solvents. The oxidation of $L_2Ru(NCS)_2$ in CH_2Cl_2 at a platinum macrodisk electrode under conditions of cyclic voltammetry is shown in Figure 10. As was the case with L_2RuCl_2 in CH_3CN, a second process (not shown) with a peak current comparable to that of the initial oxidation process is observed at +1.5 V at a scan rate of 200 mV s^{-1}. This process is not fully reversible and might be a metal-centered $Ru^{III/IV}$ or

(47) Cotton, F. A.; Wilkinson, G. *Carbon: Group IVA(14)*, 5th ed.; John Wiley & Sons Inc.: New York, 1988; Chapter 8, pp 234−264.
(48) Kohle, O.; Grätzel, M.; Meyer, A. F.; Meyer, T. B., *Adv. Mater.*, **1997**, *9*, 904.
(49) Jones, E.; Munkley, C. G.; Phillips, E. D.; Stedman, G., *J. Chem. Soc., Dalton Trans.*, **1996**, 1915−1920.
(50) Lever, A. B. P. *Inorg. Chem.* **1990**, *29*, 1271−1285.

a ligand-based thiocyanate oxidation process. The cyclic voltammetric responses obtained in this noncoordinating solvent suggest the presence of a stable product since even at scan rates as low as 10 mV s^{-1} a reverse peak is found. However, careful examination of data obtained over the scan rate range of 10−5000 mV s^{-1} reveals that diffusion-controlled mass transport is not achieved because plots of i_p^{ox} and i_p^{red} versus $\upsilon^{1/2}$ are not linear (see inset Figure 10) and the peak-to-peak potential separation at slow scan rates is 48 mV, which is less than observed for the ideal model compound L_2RuCl_2 and less than expected theoretically for a one-electron process. In contrast, when the microdisk or rotating disk electrode techniques are used, the $L_2Ru(NCS)_2$ oxidation process corresponds to a chemically reversible mass transport controlled one-electron process. That is, slopes calculated from "log-plots" obtained from these techniques were 67 ± 5 mV and similar to those obtained for the one-electron oxidation of L_2RuCl_2 under the same conditions. Furthermore, data obtained from rotating disk electrode voltammograms show that a plot of i_L versus $\omega^{1/2}$ was linear and passed through the origin. From data obtained under the latter conditions values of D and $E^r_{1/2}$ may be calculated (Table 2). Cyclic voltammograms simulated using these values are compared to a recorded voltammogram in Figure 10. The substantial difference between the mass transport controlled (simulation) and the measured voltammogram can be clearly seen. Not only is the calculated half-wave potential different by 5 mV, the experimentally measured peak current is almost double that predicted by the simulation. Apparently reactant and product adsorption provide a major contribution to the cyclic voltammetric response, as is the case with oxidation of $(H_2\text{-dcbpy})_2Ru(NCS)_2$.[26]

In cyclic voltammetric studies in CH_3CN, while the peak current ratio i_p^{ox}/i_p^{red} is almost unity, the peak-to-peak separation $\Delta E_p = 40 \pm 5$ mV for scan rates between 10 and 100 mV s^{-1}, which is significantly smaller than theoretically expected for a diffusion controlled one-electron charge transfer process and as observed for the ideal L_2RuCl_2 model system. Further, i_p^{red} does not scale with $\upsilon^{1/2}$ and at fast scan rates $\upsilon > 50$ V s^{-1} i_p^{red} is almost independent of scan rate. Additionally, at −40 °C the reduction peak potential shifts to a very much more negative potential, resulting in a ΔE_p value of 240 ± 20 mV. That is, surface-based processes perturb the oxidation process as is the case in CH_2Cl_2 and for the oxidation of $(H_2\text{-dcbpy})_2Ru(NCS)_2$.[26] However, again when the microdisk electrode or the rotating disk electrode is used, the oxidation of $L_2Ru(NCS)_2$ in CH_3CN is chemically reversible and mass transport controlled as evidenced from slopes of "log-plots" of 63 ± 3 mV and plots of i_L versus $\omega^{1/2}$ which pass through the origin in the case of rotating disk electrode experiments. From these log-plots the reversible half-wave potential in CH_3CN can be calculated, and the value is listed in Table 2. Exhaustive bulk electrolysis of $L_2Ru(NCS)_2$ in CH_3CN proceeds as in DMF, with the cyanide analogue, $L_2Ru(CN)_2$, being formed.

3.5. Spectroscopic Considerations. In a recent XPS study[25] on $(H_2\text{-dcbpy})_2Ru(NCS)_2$ it was suggested that the oxidation of $(H_2\text{-dcbpy})_2Ru(NCS)_2$ might be thiocyanate based rather than metal based as assumed for other derivatives. Comparison of data with a previous study[26] shows that the reversible potential for the oxidation of $(H_2\text{-dcbpy})_2Ru(NCS)_2$ is almost unaffected upon esterification of the carboxylate groups so that potential data obtained from esters may be used as a basis for comparison. A linear relationship is found between the energy of both MLCT bands[51] and the reversible potential for the $[L_2RuX_2]^{0/+}$ process in DMF using $E_{1/2}$ values obtained from differential pulse voltammograms (lower energy band, slope 4.3×10^3 cm^{-1} V^{-1}, intercept 2.3×10^4 cm^{-1}, $r = 99.7\%$; higher energy band, slope 4.0×10^3 cm^{-1} V^{-1}, intercept 1.6×10^4 cm^{-1}, $r = 99.8\%$). The linear relationship is also obtained when CH_3CN is chosen as the solvent. No unusual feature in the value for the reversible potential for the $[L_2Ru(NCS)_2]^{0/+}$ process emerges from this comparison.

The MLCT transition reflects the relative energy levels of the metal center and the participating ligand.[33,52] In the case of the bipyridine ligands an electron from the metal σ-orbital becomes promoted into an empty π^*-bpy orbital during the transition. Since the bipyridine part stays unchanged in the L_2RuX_2 series, the change in the MLCT transfer bands should directly reflect the change in σ-orbital energy and hence the reversible oxidation potential. If the oxidation process is metal centered, the change in the MLCT transfer transitions should scale linearly with the change in oxidation potential. Thus, this linear relationship implies that it is highly likely that the oxidation of $L_2Ru(NCS)_2$ is indeed a $Ru^{II/III}$ oxidation rather than a thiocyanate ligand oxidation process.

4. Conclusions

It has emerged that L_2RuCl_2 is a model compound for voltammetric studies of the $[L_2RuX_2]^{0/+}$ redox couple. Electrochemically generated $[L_2RuCl_2]^+$ is stable on the time scale of hours and can therefore be characterized by a range of spectroscopic techniques. ESR spectra obtained from $[L_2Ru^{III}Cl_2]^+$ suggest that the symmetry of the oxidized complex is less than C_{2v}, which can be explained by assuming that distortion of the Et_2-dcbpy ligands occurs after oxidation. When more easily oxidizable halide or pseudo-halide ligands are present, the redox chemistry associated with the oxidation process becomes considerably more complicated. In the case of L_2RuI_2, electrochemical oxidation resulted in an overall internal reaction leading to loss of iodine. When coordinating solvents such as DMF and CH_3CN were used, solvent-substituted complexes were formed, whereas in noncoordinating solvents, the five-coordinate complex $[L_2RuI]^+$ was formed. The formation of these charged complexes was proven by electrospray mass spectrometry and voltammetric techniques.

The oxidation of $L_2Ru(CN)_2$ is even more complicated than that of L_2RuI_2 with mono- and polynuclear ruthenium compounds being formed. Products formed by reaction with the oxidized ligand, cyanogen $(CN)_2$, or a derivative, are believed to be involved in the complex reaction pathways.

Voltammetric oxidation of $L_2Ru(NCS)_2$ is accompanied by adsorption as is the case with the protonated acid $(H_2\text{-dcbpy})_2Ru(NCS)_2$.[26] It can be proposed that surface attachment occurs via the sulfur component of thiocyanate groups, since surface processes are absent when other halides or pseudo halides are present. Oxidation of $L_2Ru(NCS)_2$ leads to formation of the cyanide analogue $L_2Ru(CN)_2$ and appears to proceed without the formation of the mixed ligand complex $L_2Ru(NCS)(CN)$. Degradation in photovoltaic cells may also proceed via this route, since the main photoelectrochemical cycle involves the momentary oxidation of the sensitizer.[48]

Acknowledgment. The authors would like to express their thanks to Dr. David Humphrey for valuable assistance in the

(51) Wolfbauer, G.; Bond, A. M.; MacFarlane, D. R. *Inorg. Chem.*, submitted.
(52) Heath, G. A. In *Spectro-Electrochemistry and Electrochemical Spectroscopy*; Pombeiro, A. J. L., McCleverty, J. A., Eds.; Kluwer Academic Publishers: Dordrecht, The Netherlands, 1993; pp 533−547.
(53) Kohle, O.; Ruile, S.; Grätzel, M. *Inorg. Chem.* **1996**, *35*, 4779−4787.

interpretation of the electronic spectra, Dr. Leone Spiccia and Prof. Glen D. Deacon for providing the H_2-dcbpy ligand, Dr. Georgii Lazarev for recording and simulating the ESR spectra, and Drs. Lai Yoong Goh and Sue Jenkins for extensive discussions on the synthesis.

Supporting Information Available: Detailed description and discussion on the syntheses of the ligand and the complexes and their characterization by elemental analysis, FT-IR, and NMR (Section S1). Listing of ^{1}H and ^{13}C NMR shifts and couplings constants for L_2RuX_2 complexes (Table S1). Plot of energy of both MLCT bands versus the reversible oxidation potential for the $[L_2Ru^{II/III}X_2]^{0/+}$ process in DMF (Figure S1). This material is available free of charge via the Internet at http://pubs.acs.org.

IC990344U